



HAL
open science

Fluorescent detection of GDP in real time with the reagentless biosensor, rhodamine-ParM

Simone Kunzelmann, Martin R Webb

► **To cite this version:**

Simone Kunzelmann, Martin R Webb. Fluorescent detection of GDP in real time with the reagentless biosensor, rhodamine-ParM. *Biochemical Journal*, 2011, 440 (1), pp.43-49. 10.1042/BJ20110349 . hal-00642832

HAL Id: hal-00642832

<https://hal.science/hal-00642832>

Submitted on 19 Nov 2011

HAL is a multi-disciplinary open access archive for the deposit and dissemination of scientific research documents, whether they are published or not. The documents may come from teaching and research institutions in France or abroad, or from public or private research centers.

L'archive ouverte pluridisciplinaire **HAL**, est destinée au dépôt et à la diffusion de documents scientifiques de niveau recherche, publiés ou non, émanant des établissements d'enseignement et de recherche français ou étrangers, des laboratoires publics ou privés.

Fluorescent detection of GDP in real time with the reagentless biosensor, rhodamine-ParM

Simone Kunzelmann and Martin R. Webb¹

MRC National Institute for Medical Research, Mill Hill, London NW7 1AA, United Kingdom

¹To whom correspondence should be addressed (email: mwebb@nimr.mrc.ac.uk)

Short title: Fluorescent biosensor for GDP

Abbreviations used: BSA, bovine serum albumin; DTT, dithiothreitol; GEF, guanine nucleotide exchange factor; 5-IATR and 6-IATR, 5- and 6-iodoacetamidotetramethylrhodamine; 5- and 6-ATR-ParM, adduct of a ParM mutant with 5-IATR or 6-IATR; TCEP, tris(2-carboxyethyl)phosphine; MDCC, *N*-[2-(1-maleimidyl)ethyl]-7-diethylaminocoumarin-3-carboxamide

Accepted Manuscript

SYNOPSIS

The development of novel fluorescence methods for the detection of key biomolecules is of great interest, both in basic research and in drug discovery. Particularly relevant and widespread molecules in cells are ADP and GDP, which are the products of a large number of cellular reactions, including reactions catalyzed by nucleoside triphosphatases and kinases. Previously biosensors for ADP were developed in this laboratory, based on fluorophore adducts with the bacterial actin homologue ParM. It is shown here that one of these biosensors, tetramethylrhodamine-ParM, can also monitor GDP. The biosensor can be used to measure micromolar concentrations of GDP on the background of millimolar concentrations of GTP. The fluorescence response of the biosensor is fast, the response time being <0.2 s. Thus, the biosensor allows real-time measurements of GTPase and GTP-dependent kinase reactions. Applications of the GDP biosensor are exemplified with two different GTPases, measuring the rates of GTP hydrolysis and nucleotide exchange.

Key words: fluorescence, sensor, guanosine triphosphatase, GTPase, nucleotide exchange factor, rhodamine stacking

INTRODUCTION

Guanosine triphosphatases play essential roles in many cellular processes such as signal transduction, cytoskeletal reorganisation, vesicle trafficking, regulation of translation, membrane remodeling and pathogen defence [1-3]. Typically the function of GTPases relies on cycling between different protein conformations, determined by the state of the bound nucleotide, either GDP or GTP. Switching between these active and inactive states is tightly controlled by regulatory proteins that affect the rates of exchange of bound nucleotide (GDP to GTP) and GTP hydrolysis to GDP and inorganic phosphate. Mutations in GTPases or their regulators that interfere with the GTPase cycle cause a number of human diseases, an example being the frequent involvement of Ras-related GTPases in human cancer [4]. Assays to measure the activity of GTPases are therefore of great interest for basic research as well as drug discovery.

Fluorescent, reagentless biosensors are widely used tools for the detection and quantitative measurement of biological important molecules and hence for reporting biological activity. They consist of a biomolecule (protein, DNA, RNA) that specifically binds the analyte and a fluorescent reporter group that couples the recognition of that analyte to a fluorescence change. Protein-based biosensors are a subgroup of reagentless biosensors, where the recognition unit is a fluorescently labeled protein or protein domain. Examples include biosensors for inorganic phosphate, sugars, amino acids, cations such as Ca^{2+} , nucleotides and single-stranded DNA [5-10]. These types of biosensors offer a number of advantages. First, the signal change can be very fast, limited only by the speed of ligand binding to the protein or the associated conformational change. Hence they can be used for real-time measurements of enzyme activity. Second, the protein-ligand interaction can provide high specificity. Finally a key feature of reagentless biosensors is that only a single component, the labeled protein, is needed for detection, thereby minimizing interference with the system under study.

Fluorescent biosensors for ADP were previously developed by engineering ParM, an actin homologue from bacteria that is involved in plasmid segregation [11, 12]. The design of the biosensor relies on a large conformational change of ParM that occurs on nucleotide binding: the two subdomains of the actin-fold rotate against each other by 25° , thereby closing the nucleotide binding site located in a cleft between them [13]. This conformational change was coupled to an optical signal first by introducing cysteine residues at specific locations near the rim of the binding cleft. These cysteines provide specific sites to couple with thiol-reactive probes (maleimides or iodoacetamides) [14]. The fluorophores were placed such that their fluorescence responds to the conformation change on ADP binding. Two distinct versions with different properties were produced using either a coumarin, MDCC [11], or a tetramethylrhodamine [12] as the reporter. The coumarin version makes use of the environmental sensitivity of the signal of the single fluorophore.

In contrast, the rhodamine version is achieved by labeling two cysteine residues of a ParM mutant with either 5- or 6-iodoacetamidotetramethylrhodamine (5- or 6-IATR) (Figure S1). The two labeling sites are located on the two different subdomains, either side of the binding cleft. In the nucleotide-free state the two rhodamines are in close proximity and are likely to form a stacking interaction that largely quenches their fluorescence [15]. Nucleotide binding causes an increase in fluorescence, probably by disturbing the stacking interaction of the rhodamines. In addition to introducing the cysteine residues for label attachment, other mutations were introduced to enhance discrimination against nucleoside triphosphate binding and prevent the ParM polymerizing, so it remains a monomer [11, 12]. The final protein used for this rhodamine-labeled biosensor is (His₆/K33A/D63C/T174A/T175N/D224C/C287A) ParM [12].

It is demonstrated here that the tetramethylrhodamine-labeled ParM is also suitable for the detection of other nucleoside diphosphates including GDP, thus providing a novel method to measure the activity of GTPases and other enzymes that produce GDP. The biosensor is characterized for its interaction with guanine and other nucleotides. Example assays demonstrate the use of the biosensor to assay GDP release by enzymes following GTP hydrolysis or due to nucleotide exchange.

EXPERIMENTAL

ParM expression, purification and labeling with IATR

The ParM construct for rhodamine labeling, ParM (His₆/K33A/D63C/T174A/T175N/D224C/C287A), was generated from vector pJSC1 containing ParM wildtype [16] by site-directed mutagenesis (Stratagene) [12]. The identity of the construct was verified by DNA sequencing. The protein construct comprises full length ParM (amino acids 1-320) plus an additional 10aa peptide (QSGSHHHHHH) at the C-terminus. Expression was performed in BL21-Ai cells (Invitrogen) as described [12]. ParM expression cultures were grown at 30 °C in 2x TY medium containing 100 µg ml⁻¹ ampicillin until the optical density at 600 nm was 0.4-0.6 cm⁻¹, when overexpression was induced by addition of 2 mg L⁻¹ arabinose. Cells were harvested after 16 h induction, resuspended in lysis buffer (30 mM Tris-HCl pH 8.0, 25 mM KCl, 1 mM tris(2-carboxyethyl)phosphine (TCEP) 0.1% Triton X-100) and stored at -80 °C. His-tagged ParM was then purified by Ni-chelate chromatography. Cleared cell extracts were supplemented with 500 mM NaCl and filtered through a 0.45 µm syringe filter (Sartorius). The lysate was loaded onto a 5 ml HisTrap HP column (GE Healthcare), equilibrated with buffer A (30 mM Tris-HCl pH 8.0, 500 mM NaCl, 1 mM TCEP). The column was washed with buffer A until the absorbance at 280 nm reached the baseline, followed by 50 mL buffer B (30 mM Tris-HCl pH 8.0, 25 mM KCl, 1 mM TCEP). ParM was eluted with a 100 mL linear gradient of 0-250 mM imidazole in buffer B, adjusted to pH 8.0. Fractions containing ParM were pooled and 10 mM DTT was added. Protein solutions were concentrated using a Vivaspinn-20 centrifugal concentrator (Vivascience) and then further purified over a HiLoad Superdex 75 column (26/60, GE Healthcare) equilibrated in 30 mM Tris-HCl pH 7.5, 25 mM KCl, 1 mM EDTA and 5 mM DTT. Fractions containing monomeric ParM were pooled and concentrated again as above. The concentration of ParM mutants was determined by absorbance measurements using the extinction coefficient 34,380 M⁻¹cm⁻¹ at 280 nm, calculated from the primary sequence [17]. Proteins were shock-frozen in liquid nitrogen and stored at -80 °C.

The ParM construct contains two exposed cysteines (C63 and C224) that are accessible to modification with thiol-reactive iodoacetamide probes. A third cysteine in the construct (C100) is buried in the core of the structure and not readily accessible to labelling (see below). Labeling of ParM with 5- or 6-iodoacetamidotetramethylrhodamine (IATR) [18] was performed as described previously [12]. In brief, DTT was removed from ParM solutions using a PD10 column (GE Healthcare) and ParM was labeled with IATR at four-fold molar excess for 90 min at room temperature in 30 mM Tris-HCl pH 7.5, 25 mM KCl. The reaction was stopped by the addition of 2-mercaptoethanesulfonate, that captures the unreacted IATR. Free fluorophore was removed on a PD10 column. Labeled ParM was further purified by anion exchange chromatography on a HiTrapQ HP column (GE Healthcare) using a gradient of 25mM to 200 mM KCl. The protein was concentrated in an Amicon Ultracentrifugal filter device (Millipore Corporation), shock-frozen in liquid nitrogen and stored at -80°C. Concentration of tetramethylrhodamine-labeled ParM mutants were determined from the absorbance spectra using the extinction coefficient of a small molecule thiol adduct of 5-IATR at its isosbestic point, $\epsilon_{528} = 52,000 \text{ M}^{-1}\text{cm}^{-1}$ [19]. The labeling stoichiometry of two labels per protein molecule was confirmed by electrospray ionization mass spectrometry.

Nucleotides

All nucleotides were purchased from Sigma-Aldrich at the highest purity available. GTP was purified further by anion-exchange chromatography and its purity was analyzed by HPLC as described [11]. Nucleotide concentrations were determined from their absorbance spectra in 20 mM Tris-HCl pH 7.5 using the extinction coefficients $\epsilon_{253} = 13,700 \text{ cm}^{-1}$ for guanine, $\epsilon_{259} = 15,400 \text{ cm}^{-1}$ for adenine, $\epsilon_{260} = 9,900 \text{ cm}^{-1}$ for uracil, $\epsilon_{260} = 6,100 \text{ cm}^{-1}$ for cytosine and $\epsilon_{260} = 8,700 \text{ cm}^{-1}$ for thymidine nucleotides.

Fluorescence titrations

Equilibrium fluorescence measurements were performed using a Cary Eclipse fluorescence spectrophotometer (Varian). 0.5 μM 5- or 6-ATR-ParM was titrated with different nucleotides and the rhodamine fluorescence was recorded at 577 nm after excitation at 553 nm. Data were analyzed by fitting hyperbolic curves using the program GraFit 5.0. Titrations were done in 30 mM Tris-HCl pH 7.5, 25 mM KCl, 3 mM MgCl_2 and 5 μM BSA at 20 °C.

Stopped-flow fluorescence experiments

Stopped-flow measurements were performed using a HiTech SF61 DX2 stopped-flow instrument equipped with a Xe/Hg lamp (TgK Scientific, UK). Association kinetics of 5- and 6-ATR-ParM and GDP were measured under pseudo-first order conditions with excess of GDP over ParM. Tetramethylrhodamine fluorescence was excited at 546 nm and emission was detected with a photomultiplier after filtering emitted light through a 570 nm long-pass filter. Experimental traces were analyzed by single exponential curve fitting using the HiTech software. All measurements were performed at 20 °C in 30 mM Tris-HCl pH 7.5, 25 mM KCl, 3 mM MgCl_2 and 5 μM BSA.

GTP hydrolysis assay

Steady-state kinetics of GTP hydrolysis by hGBP5a/b [20] were measured in 50 mM Tris-HCl pH 8.0, 25 mM KCl, 5 mM MgCl_2 , 2 mM DTT and 5 μM BSA at 25 °C using a Cary Eclipse fluorescence spectrophotometer (Varian). Different concentrations of GTP (0-1 mM) and 5-ATR-ParM (0.25 μM final concentration) were incubated in the cuvette at 25 °C and the reaction was started by the addition of hGBP5 (0.22 μM final concentration). Rhodamine fluorescence was excited at 553 nm and detected at 577 nm. The fluorescence response of 5-ATR-ParM was calibrated by titrating ParM with a GDP standard solution in the presence of 0, 0.5 and 1 mM GTP. Data were analyzed by linear regression. The slope of the calibration was dependent on the GTP concentration present, albeit the difference was small: about 10% difference between 0 and 1 mM GTP. Assuming a linear relationship between the slope of the calibration curve and [GTP], for each [GTP] used in the assay a slope was calculated by linear interpolation. These were used to convert the measured fluorescence time traces to the time course of GDP formation. Initial rates were determined by linear fitting to the data points with less than 10% of the GTP turned over. Michaelis-Menten plots (Initial rate versus [GTP]) were generated and analyzed by hyperbolic curve fitting using GraFit 5.0 [21].

Nucleotide exchange assays

Nucleotide exchange of H-Ras was measured in 20 mM HEPES pH 7.4, 150 mM KCl, 5 mM MgCl_2 , 2 mM DTT and 5 μM BSA at 25 °C using a Cary Eclipse fluorescence spectrophotometer (Varian). GDP-bound Ras (Ras-GDP) and 5-ATR-ParM (concentrations given in the legend of Figure 5) were incubated at 25 °C in the cuvette and the exchange reaction was started by adding 1 mM GTP and/or the catalytic domain of Sos (residues 564-1049, Sos^{cat}) [22]. Fluorescence was recorded at excitation and emission wavelengths of 553 nm and 577 nm, respectively. The biosensor response was calibrated as described for the GTPase assay above, but using the calibration in the presence of 1 mM GTP for all data to calculate GDP concentrations from the fluorescence signal. Data points up to maximally 10% turnover were analyzed to obtain initial rates by linear regression. Initial rates were plotted as a function of Ras-GDP concentration and hyperbolic curve fitting was performed with GraFit 5.0 [21].

RESULTS AND DISCUSSION

Native ParM, the protein scaffold of the ADP biosensors previously described, binds guanine nucleotides in addition to adenine nucleotides [23]. The coumarin-labeled biosensor, MDCC-ParM, binds GDP but does not exhibit a fluorescence change [11], so this version is not suitable for GDP

detection. In contrast, both isomers of the tetramethylrhodamine-based biosensor, 5- and 6-ATR-ParM (His₆/K33A/D63C/T174A/T175N/D224C/C287A), respond to GDP binding with a ~10-fold increase in fluorescence (Figure 1, Table 1). Before describing the application of the double rhodamine, ParM-based biosensor to GDP measurement, the precise identity of this molecule is considered.

The substitution reactions of iodoacetates and iodoacetamides are very selective for thiols (such as in cysteine residues) [14, 24-26], although they can also react with methionine, tyrosine, histidine and lysine. This is, in part, due to the much larger nucleophilicity of thiol over other available groups on a protein that could take part in the nucleophilic substitution reaction [27] (Figure S1). Under conditions of neutral pH, ambient temperature and limited excess of iodoacetamide over thiols, the reaction with cysteine is orders of magnitude faster than reaction with any other amino acid [14, 24-29]. The ParM construct, described here (His₆/K33A/D63C/T174A/T175N/D224C/C287A), contains two exposed cysteines (C63 and C224) that, according to the known crystal structures, are accessible to modification. Indeed, they were added for that purpose. A third, wild-type cysteine in the construct (C100) is buried in the core of the structure and so is unlikely to be modified. Mass spectrometry showed that each molecule of this construct is labeled with two acetamidotetramethylrhodamine moieties [12]. In order to confirm that the two labels are on the two exposed cysteine residues, two mutants were constructed with only one exposed cysteine present, ParM (His₆/K33A/D63A/T174A/T175N/D224C/C287A) and ParM (His₆/K33A/D63C/T174A/T175N/D224A/C287A), as well as one mutant where both exposed cysteines were removed, ParM (His₆/K33A/D63A/T174A/T175N/D224A/C287A). These proteins were reacted with 5-IATR under the same conditions as the biosensor construct and analyzed by electrospray ionization mass spectrometry (Figure S2) and absorbance spectroscopy (Figure S3). Both mutants with only one exposed cysteine (63A/224C and 63C/224A) reacted with only one 5-IATR molecule per protein (Table S1). The mutant that had both cysteines removed (63A/224A) showed only a very small fraction of labeling (~4% of the protein, Figure S3) and the majority (96%) was unlabeled. Thus the two labels on the biosensor are on the cysteine residues, C63 and C224, introduced for this purpose. It is possible that a small fraction (<5%) of the protein has some unspecific labeling on other amino acids, but importantly this is unlikely to impair the biosensor function.

As previously shown for ADP, 5- and 6-ATR-ParM behave very similarly to each other with other nucleoside diphosphates in terms of affinity, kinetics and signal change. In the following, characterization of the 5-isomer is described and then the similarities and differences of 6-ATR-ParM are summarized.

A titration of GDP with 5-ATR-ParM, measuring fluorescence, shows that this nucleotide binds only slightly weaker than ADP (2.5-fold) (Table 1). The dissociation constant was determined as 75 μ M in a buffer containing 25 mM KCl. The GDP affinity is about two-fold higher at 150 mM potassium chloride. The biosensor strongly discriminates between GDP and GTP (Figure 1). GTP binds much weaker than GDP and shows only a small fluorescence increase. The sensitivity of ATR-ParM is more than 100-fold higher for GDP than for GTP: while 10 μ M GDP causes a >2-fold change in fluorescence, >1 mM GTP is needed to produce the same change (Figure 1). These data suggest that 5-ATR-ParM is well suited for sensing GDP in the presence of GTP. At nucleotide concentrations higher than those shown in Figure 2 the fluorescence decreases after reaching a maximum. However, this is outside the concentration range of possible GDP measurements due to saturation of the biosensor and therefore does not affect the biosensor performance.

ATR-ParM also responds to other nucleoside diphosphates (dADP, dGDP, CDP, dCDP, TDP and UDP) with a fluorescence increase upon binding that ranges between 9-fold and 14-fold (Table 1). Except for CDP and dCDP, which bind considerably weaker ($K_d > 700 \mu$ M), the dissociation constants of the other nucleotides are in the same range as GDP and ADP (28-105 μ M).

In order to assess if the biosensor is suitable for real-time monitoring of GDP formation, the kinetics of GDP binding were determined using stopped-flow (Figure 2). Binding kinetics were measured under pseudo-first-order conditions with excess GDP over 5-ATR-ParM. Time courses

show that GDP binding is fast, completed in <1 s even at the lowest concentration of GDP (Figure 2a). The fluorescence traces are well described by single exponentials. The observed rate constants show a linear dependence on the concentration of GDP indicating that the speed of the fluorescence response in the concentration range measured is controlled by the bimolecular binding step rather than a conformational change (Figure 2b). Association (k_{on}) and dissociation rate constants (k_{off}) obtained from linear regression are $0.047 \mu\text{M}^{-1}\text{s}^{-1}$ and 4.8 s^{-1} , respectively. The slightly lower affinity of the biosensor for GDP in comparison to ADP [12] is mainly due to a lower k_{on} value, whereas the k_{off} value is very similar. The dissociation constant obtained from the kinetics ($K_{\text{d}} = k_{\text{off}}/k_{\text{on}}$) is $103 \mu\text{M}$, which is in reasonable agreement with the value from equilibrium titrations. Given that the fluorescence response of the biosensor to GDP occurs with rate constant $k_{\text{off}} + k_{\text{on}}[\text{GDP}]$, this response is always greater than k_{off} (4.8 s^{-1}). This corresponds to a response time of <200 ms ($1/k_{\text{off}}$). Thus, the biosensor is well suited for real-time measurements of GDP in steady-state or slow transient kinetic assays using manual mixing. In order to observe “pure” GDP release rate constants using fast kinetic techniques (e.g. stopped-flow), this rate constant needs to be ~ 10 -fold slower than the biosensor response, corresponding to a release rate constants of $<0.5 \text{ s}^{-1}$.

The performance of the GDP biosensor was tested in real-time assays by measuring the steady-state GTPase activity of human guanylate binding protein 5 (hGBP5). hGBP5 is a mammalian, dynamin-related GTPase that is induced by interferons, shows tumor-associated expression and has a role in innate immunity [3, 30]. GTP hydrolysis by hGBP5 was measured at different GTP concentrations by monitoring GDP formation using 5-ATR-ParM (Figure 3). To calibrate the fluorescence response, 5-ATR-ParM was titrated with GDP in the presence of different concentrations of GTP under the assay conditions (Figure 3a). The fluorescence response was linearly dependent on GDP up to $\sim 20 \mu\text{M}$. The presence of GTP had only a small effect on the slope of the calibration: $<10\%$ difference was observed between 0 and 1 mM GTP. The calibration accounted for this as described in the Experimental section. Fluorescence time courses were converted to GDP concentrations and initial rates were determined by linear regression (Figure 3b, inset). Michaelis-Menten plots of initial rates versus GTP concentration gave the parameters $K_{\text{M}} = 79 \mu\text{M}$ and $v_{\text{max}} = 0.467 \mu\text{M min}^{-1}$ (Figure 3b). The catalytic activity (k_{cat}) of 2.1 min^{-1} , determined here, is in good agreement with a previous study, where the activity of hGBP5 was determined as 1.7 min^{-1} in an HPLC-based assay under very similar solution conditions [20].

A second application of the GDP biosensor is nucleotide exchange of the small GTPase Ras, a key signaling molecule in the regulation of cell growth, proliferation, differentiation and apoptosis [31]. Ras is activated by nucleotide exchange factors (GEFs) that convert GDP-bound Ras to GTP-bound Ras by accelerating nucleotide dissociation. Son of sevenless (Sos) is one of these Ras-specific exchange factors. Nucleotide exchange from Ras-GDP to Ras-GTP was measured using 5-ATR-ParM to monitor released GDP (Figure 4). A large excess of free GTP over Ras-GDP was used to get complete exchange of GTP for GDP, ensuring quasi-irreversible dissociation of GDP. GDP release from $10 \mu\text{M}$ Ras-GDP was very slow in the absence of nucleotide exchange factor and strongly accelerated by addition of the catalytic domain of Sos (Sos^{cat}) (Figure 4a). If there was no GTP present to replace the dissociating GDP, net release of GDP was not detectable. (Figure 5a). This finding indicates that Sos alone cannot displace GDP from Ras. In other words, the nucleotide-free complex of Ras and exchange factor (Sos-Ras) is not formed in significant amounts ($<5\%$) under these conditions. The apparent half times of the exchange reaction were 240 s, 80 s, 25 s and 2.5 s at 0.1, 0.3, 1 and $10 \mu\text{M}$ Sos^{cat} , respectively. Under single turnover conditions ($10 \mu\text{M}$ Sos^{cat} , $10 \mu\text{M}$ Ras-GDP) the apparent rate constant obtained from single exponential curve fitting was 0.28 s^{-1} . This is >10 -fold faster than the single turnover rate constant reported previously at the same concentration of Sos^{cat} but lower Ras-GDP ($1 \mu\text{M}$) [32, 33]. The large difference could be explained by the allosteric feedback mechanism governing Sos-catalyzed nucleotide exchange [34]. Beside the catalytic Ras binding site Sos^{cat} possesses a second interaction site, where Ras-GTP and, to a lesser extent, Ras-GDP binding causes an allosteric activation of Sos catalytic activity [34]. A higher concentration of Ras might lead to a higher occupation of this allosteric site and thus faster nucleotide exchange. In addition, the use of fluorescently labeled mantGDP in the studies of Ford et

al [32, 33] might also contribute to the observed difference in rate constants, because nucleotide dissociation from Ras is slower for mant-nucleotides than for unlabeled nucleotides [35].

Nucleotide exchange of the same system was measured under steady-state conditions using a constant, low concentration of Sos^{cat} and increasing concentrations of Ras-GDP (Figure 4b). The initial rate of GDP dissociation increased with Ras-GDP concentration with approximately hyperbolic dependence. Although the data do not allow an accurate determination of the Michaelis-Menten parameters since saturation is not reached, lower limits can be estimated for $K_M > 400 \mu\text{M}$ and $k_{\text{cat}} > 20 \text{ s}^{-1}$. Such a high apparent K_M value has also been observed for the related Ras GEF, Cdc25^{Mm} ($K_M = 386 \mu\text{M}$) [36]. The intrinsic exchange rate for Ras-GDP, determined with the GDP biosensor, was $3.6 \times 10^{-5} \text{ s}^{-1}$ (data not shown) in agreement with previous studies [33, 36]. Thus, nucleotide exchange is accelerated by Sos^{cat} by more than five orders of magnitude as found for many GEFs of small GTPases [37].

So far, the 5-isomer of ATR-ParM has been described for its use as a biosensor for nucleoside diphosphates, in particular GDP. Generally the ParM version, labeled with the 6-ATR, behaves very similarly to 5-ATR-ParM with respect to NDP and dNDP binding (Table 1 and 2, Figure 2 and 3). 6-ATR-ParM shows a similar fluorescence response as 5-ATR-ParM to the different nucleoside diphosphates, with slightly lower affinity for NDPs including GDP and similar binding kinetics. Hence, 6-ATR-ParM can be used in the same way as 5-ATR-ParM to measure nucleoside diphosphates.

In summary, 5-ATR-ParM and 6-ATR-ParM function as biosensors for GDP that can be used to measure rates of GTP hydrolysis and nucleotide exchange of GTPases. This is a wide ranging group of enzymes, including small G-proteins, heterotrimeric G proteins, GTPases involved in transcription and translation, and large, dynamin-related GTPases. GTP-dependent kinases are another group of enzymes that could be studied with these biosensors, albeit they are less in number than GTPases. These kinases, for example phosphoenolpyruvate carboxykinase transfer the γ -phosphate of GTP onto a substrate thereby releasing GDP. In addition there are other metabolic enzymes that produce GDP, such as a variety of enzymes that handle GDP-sugars, for example transferases involved in carbohydrate biosynthetic pathways, as well as specific examples, GDP-L-galactose phosphorylase and GDP-mannose glycosyl hydrolase.

ATR-ParM shows a fast fluorescence response (<200 ms response time) allowing real-time measurements of GDP concentration changes on the time scale of seconds. The biosensor has micromolar sensitivity for GDP and discriminates well against GTP. The dynamic range for GDP detection, estimated from the concentrations at 10% and 90% saturation, is 5-500 μM in Tris buffer pH 7.5, 150 mM KCl. These upper and lower limits depend on the exact buffer conditions and will be shifted, e.g by ionic strength, pH value and temperature, according to the GDP dissociation constant. The fluorescence response of the biosensor is approximately linear at concentrations well below the K_d value, whereas at higher concentrations a hyperbolic equation can be used for calibration. The contribution of GTP binding to the signal is negligible (<5%) at concentrations up to $\sim 800 \mu\text{M}$ (Figure 1) but can be corrected by appropriate calibrations, if high accuracy or higher concentrations of GTP are needed. In practice, the biosensor is able to detect down to 2 micromolar concentrations of GDP in the presence of millimolar GTP as demonstrated in the GTPase and nucleotide exchange assays (Figures 4 and 5). The broad specificity for nucleoside diphosphates and deoxynucleoside diphosphates enables the biosensor to be used for measuring reactions that release other diphosphates, in addition to ADP and GDP. On the other hand, due to the similar affinities of the biosensor for the NDPs, the presence of any other diphosphate in addition to the one to be studied would interfere with the detection, unless its concentration is much lower than its K_d for the biosensor. Further engineering of the active site by site-directed mutagenesis could potentially create new variant biosensors with higher specificity for particular diphosphates.

To our knowledge there is only one earlier described reagentless biosensor for GDP, consisting of a coumarin-labeled nucleoside diphosphate kinase [38]. That biosensor is also not specific for the base and can be used to detect all NDPs and dNDPs. However, it does not report the absolute concentration of NDP but the ratio of diphosphate to triphosphate. The reason is that the

fluorescence reports not on nucleotide binding, but on the phosphorylation state of nucleoside diphosphate kinase, which is controlled by the NTP/NDP ratio. An antibody-based assay has been described, aimed at high-throughput assays and using fluorescence polarization [39]. Other commonly used methods for measurement *in vitro* of nucleotide binding and GTP hydrolysis employ either radioactive nucleotides, HPLC analysis of labeled or unlabeled nucleotides or measurement of released inorganic phosphate (P_i) from the GTPase. For P_i measurement, there are colorimetric assays, e.g. malachite green [40, 41], coupled enzyme assays, for example using purine nucleoside phosphorylase [42, 43], and phosphate biosensors [5, 44, 45]. However, only the coupled enzyme and biosensor assays can be used in a real-time format but they are not applicable to measure guanine nucleotide exchange. The other methods require stopping the reaction at different time points to analyze individual samples, a process that can be laborious and time consuming, especially if long separation protocols are required. While assays based on absorbance detection can have comparable sensitivity to the GDP biosensor (low micromolar concentrations), radioactive assays are generally much more sensitive but they require special equipment and safety precautions. A large number of fluorescence-based assays rely on fluorescently labeled nucleotides, for example [36, 46-48] and there are also studies where labeled GTPases or regulatory proteins are used, for example [49, 50]. These methods are sensitive (possibly down to tens of nanomolar) and are particularly useful for transient kinetic studies. However, one drawback is that they require modification of the natural nucleotide or protein and thus potentially disturb the system under study. In addition, these assays are not truly generic and in particular with labeled GTPases, an assay has to be developed for each GTPase.

In conclusion, this biosensor for GDP provides a novel, generic method to measure hydrolysis activity and guanine nucleotide exchange of GTPases, or the activity of GTP-dependent kinases. This method can be used for functional and mechanistic studies on such systems, but may also find application in high-throughput screening of inhibitors for this important protein class.

ACKNOWLEDGEMENTS

We thank Mark Wehner, Dr Daniel Filchtinski and Dr Christian Herrmann (Ruhr-University Bochum, Germany) for the gifts of purified hGBP5 and H-Ras and Dr Nicolas Nassar (Stony Brook University, New York, USA) for the purified protein Sos^{cat}. We also thank Gordon Reid (NIMR, London, UK) for technical assistance.

FUNDING

This work was supported by Medical Research Council Technology and by the Medical Research Council, UK (ref. U117512742).

REFERENCES

- 1 Bourne, H. R., Sanders, D. A. and McCormick, F. (1990) The GTPase superfamily: a conserved switch for diverse cell functions. *Nature*. **348**, 125-132
- 2 Praefcke, G. J. and McMahon, H. T. (2004) The dynamin superfamily: universal membrane tubulation and fission molecules? *Nat Rev Mol Cell Biol*. **5**, 133-147
- 3 Shenoy, A. R., Kim, B. H., Choi, H. P., Matsuzawa, T., Tiwari, S. and MacMicking, J. D. (2007) Emerging themes in IFN-gamma-induced macrophage immunity by the p47 and p65 GTPase families. *Immunobiology*. **212**, 771-784
- 4 Barbacid, M. (1987) ras genes. *Annu Rev Biochem*. **56**, 779-827
- 5 Brune, M., Hunter, J. L., Corrie, J. E. and Webb, M. R. (1994) Direct, real-time measurement of rapid inorganic phosphate release using a novel fluorescent probe and its application to actomyosin subfragment 1 ATPase. *Biochemistry*. **33**, 8262-8271

- 6 de Lorimier, R. M., Smith, J. J., Dwyer, M. A., Looger, L. L., Sali, K. M., Paavola, C. D., Rizk, S. S., Sadigov, S., Conrad, D. W., Loew, L. and Hellinga, H. W. (2002) Construction of a fluorescent biosensor family. *Protein Sci.* **11**, 2655-2675
- 7 Zou, J., Hofer, A. M., Lurtz, M. M., Gadda, G., Ellis, A. L., Chen, N., Huang, Y., Holder, A., Ye, Y., Louis, C. F., Welshhans, K., Rehder, V. and Yang, J. J. (2007) Developing sensors for real-time measurement of high Ca²⁺ concentrations. *Biochemistry.* **46**, 12275-12288
- 8 Berg, J., Hung, Y. P. and Yellen, G. (2009) A genetically encoded fluorescent reporter of ATP:ADP ratio. *Nat Methods.* **6**, 161-166
- 9 Imamura, H., Nhat, K. P., Togawa, H., Saito, K., Iino, R., Kato-Yamada, Y., Nagai, T. and Noji, H. (2009) Visualization of ATP levels inside single living cells with fluorescence resonance energy transfer-based genetically encoded indicators. *Proc Natl Acad Sci U S A.* **106**, 15651-15656
- 10 Dillingham, M. S., Tibbles, K. L., Hunter, J. L., Bell, J. C., Kowalczykowski, S. C. and Webb, M. R. (2008) Fluorescent single-stranded DNA binding protein as a probe for sensitive, real-time assays of helicase activity. *Biophys J.* **95**, 3330-3339
- 11 Kunzelmann, S. and Webb, M. R. (2009) A biosensor for fluorescent determination of ADP with high time resolution. *J Biol Chem.* **284**, 33130-33138
- 12 Kunzelmann, S. and Webb, M. R. (2010) A fluorescent, reagentless biosensor for ADP based on tetramethylrhodamine-labeled ParM. *ACS Chem Biol.* **5**, 415-425
- 13 van den Ent, F., Moller-Jensen, J., Amos, L. A., Gerdes, K. and Lowe, J. (2002) F-actin-like filaments formed by plasmid segregation protein ParM. *Embo J.* **21**, 6935-6943
- 14 Johnson, I. and Spence, M. T. Z. (2010) *The Molecular Probes Handbook.* Life Technologies Corporation
- 15 Selwyn, J. E. and Steinfeld, J. I. (1972) Aggregation of equilibria of xanthene dyes. *J Phys Chem.* **76**, 762-774
- 16 Salje, J. and Lowe, J. (2008) Bacterial actin: architecture of the ParMRC plasmid DNA partitioning complex. *Embo J*
- 17 Pace, C. N., Vajdos, F., Fee, L., Grimsley, G. and Gray, T. (1995) How to measure and predict the molar absorption coefficient of a protein. *Protein Sci.* **4**, 2411-2423
- 18 Munasinghe, V. R. N. and Corrie, J. E. T. (2006) Optimised synthesis of 6-iodoacetamidotetramethylrhodamine. *ARKIVOC.* (ii), 143-149
- 19 Corrie, J. E. T. and Craik, J. S. (1994) Synthesis and characterisation of pure isomers of iodoacetamidotetramethylrhodamine. *Journal of the Chemical Society, Perkin Transactions I*, 2967-2973
- 20 Wehner, M. and Herrmann, C. (2010) Biochemical properties of the human guanylate binding protein 5 and a tumor-specific truncated splice variant. *Febs J.* **277**, 1597-1605
- 21 Leatherbarrow, R. J. (2001) *Grafit Version 5.* Erithacus Software Ltd., Horley, U.K.
- 22 Ford, B., Hornak, V., Kleinman, H. and Nassar, N. (2006) Structure of a transient intermediate for GTP hydrolysis by ras. *Structure.* **14**, 427-436
- 23 Popp, D., Narita, A., Oda, T., Fujisawa, T., Matsuo, H., Nitani, Y., Iwasa, M., Maeda, K., Onishi, H. and Maeda, Y. (2008) Molecular structure of the ParM polymer and the mechanism leading to its nucleotide-driven dynamic instability. *Embo J.* **27**, 570-579
- 24 Crestfield, A. M., Moore, S. and Stein, W. H. (1963) The Preparation and Enzymatic Hydrolysis of Reduced and S-Carboxymethylated Proteins. *Journal of Biological Chemistry.* **238**, 622-627
- 25 Glazer, A. N. (1976) Chemical modification of proteins. In *The Proteins, Vol. II* (Neurath, H., ed.). pp. 1-103, Academic Press, New York
- 26 Gurd, F. R. N. (1967) Carboxymethylation. In *Methods in Enzymology* (Hirs, C. H. W., ed.). pp. 532-541, Academic Press
- 27 Way, J. C. (2000) Covalent modification as a strategy to block protein-protein interactions with small-molecule drugs. *Current Opinion in Chemical Biology.* **4**, 40-46
- 28 Means, G. E. and Feeny, R. E. (1971) Chemical modification of proteins. In *Chemical modification of proteins.* pp. 105-110, Holden-Day, Inc. Chemical modification of proteins

- 29 Sippel, T. O. (1981) New fluorochromes for thiols: maleimide and iodoacetamide derivatives of a 3-phenylcoumarin fluorophore. *J Histochem Cytochem.* **29**, 314-316
- 30 Fellenberg, F., Hartmann, T. B., Dummer, R., Usener, D., Schadendorf, D. and Eichmuller, S. (2004) GBP-5 splicing variants: New guanylate-binding proteins with tumor-associated expression and antigenicity. *J Invest Dermatol.* **122**, 1510-1517
- 31 Vojtek, A. B. and Der, C. J. (1998) Increasing complexity of the Ras signaling pathway. *J Biol Chem.* **273**, 19925-19928
- 32 Ford, B., Skowronek, K., Boykevisch, S., Bar-Sagi, D. and Nassar, N. (2005) Structure of the G60A mutant of Ras: implications for the dominant negative effect. *J Biol Chem.* **280**, 25697-25705
- 33 Ford, B., Boykevisch, S., Zhao, C., Kunzelmann, S., Bar-Sagi, D., Herrmann, C. and Nassar, N. (2009) Characterization of a Ras mutant with identical GDP- and GTP-bound structures. *Biochemistry.* **48**, 11449-11457
- 34 Margarit, S. M., Sondermann, H., Hall, B. E., Nagar, B., Hoelz, A., Pirruccello, M., Bar-Sagi, D. and Kuriyan, J. (2003) Structural evidence for feedback activation by Ras.GTP of the Ras-specific nucleotide exchange factor SOS. *Cell.* **112**, 685-695
- 35 Neal, S. E., Eccleston, J. F. and Webb, M. R. (1990) Hydrolysis of GTP by p21NRAS, the NRAS protooncogene product, is accompanied by a conformational change in the wild-type protein: use of a single fluorescent probe at the catalytic site. *Proc Natl Acad Sci U S A.* **87**, 3562-3565
- 36 Lenzen, C., Cool, R. H., Prinz, H., Kuhlmann, J. and Wittinghofer, A. (1998) Kinetic analysis by fluorescence of the interaction between Ras and the catalytic domain of the guanine nucleotide exchange factor Cdc25Mm. *Biochemistry.* **37**, 7420-7430
- 37 Vetter, I. R. and Wittinghofer, A. (2001) The guanine nucleotide-binding switch in three dimensions. *Science.* **294**, 1299-1304
- 38 Brune, M., Corrie, J. E. and Webb, M. R. (2001) A fluorescent sensor of the phosphorylation state of nucleoside diphosphate kinase and its use to monitor nucleoside diphosphate concentrations in real time. *Biochemistry.* **40**, 5087-5094
- 39 Zielinski, T., Kimple, A. J., Hutsell, S. Q., Koeff, M. D., Siderovski, D. P. and Lowery, R. G. (2009) Two Galpha(i1) rate-modifying mutations act in concert to allow receptor-independent, steady-state measurements of RGS protein activity. *J Biomol Screen.* **14**, 1195-1206
- 40 Itaya, K. and Ui, M. (1966) A new micromethod for the colorimetric determination of inorganic phosphate. *Clin Chim Acta.* **14**, 361-366
- 41 Quan, A. and Robinson, P. J. (2005) Rapid purification of native dynamin I and colorimetric GTPase assay. *Methods Enzymol.* **404**, 556-569
- 42 Webb, M. R. (1992) A continuous spectrophotometric assay for inorganic phosphate and for measuring phosphate release kinetics in biological systems. *Proc Natl Acad Sci U S A.* **89**, 4884-4887
- 43 Webb, M. R. and Hunter, J. L. (1992) Interaction of GTPase-activating protein with p21ras, measured using a continuous assay for inorganic phosphate release. *Biochem J.* **287** 555-559
- 44 Nixon, A. E., Brune, M., Lowe, P. N. and Webb, M. R. (1995) Kinetics of inorganic phosphate release during the interaction of p21ras with the GTPase-activating proteins, p120-GAP and neurofibromin. *Biochemistry.* **34**, 15592-15598
- 45 Binns, D. D., Helms, M. K., Barylko, B., Davis, C. T., Jameson, D. M., Albanesi, J. P. and Eccleston, J. F. (2000) The mechanism of GTP hydrolysis by dynamin II: a transient kinetic study. *Biochemistry.* **39**, 7188-7196
- 46 Eccleston, J. F., Gratton, E. and Jameson, D. M. (1987) Interaction of a fluorescent analogue of GDP with elongation factor Tu: steady-state and time-resolved fluorescence studies. *Biochemistry.* **26**, 3902-3907
- 47 John, J., Sohmen, R., Feuerstein, J., Linke, R., Wittinghofer, A. and Goody, R. S. (1990) Kinetics of interaction of nucleotides with nucleotide-free H-ras p21. *Biochemistry.* **29**, 6058-6065

- 48 Kunzelmann, S., Praefcke, G. J. and Herrmann, C. (2005) Nucleotide binding and self-stimulated GTPase activity of human guanylate-binding protein 1 (hGBP1). *Methods Enzymol.* **404**, 512-527
- 49 Kraemer, A., Brinkmann, T., Plettner, I., Goody, R. and Wittinghofer, A. (2002) Fluorescently labelled guanine nucleotide binding proteins to analyse elementary steps of GAP-catalysed reactions. *J Mol Biol.* **324**, 763-774
- 50 Newcombe, A. R., Stockley, R. W., Hunter, J. L. and Webb, M. R. (1999) The interaction between rac1 and its guanine nucleotide dissociation inhibitor (GDI), monitored by a single fluorescent coumarin attached to GDI. *Biochemistry.* **38**, 6879-6886

Table 1. Affinity and fluorescence change for the binding of different nucleoside diphosphates to tetramethylrhodamine-labeled ParM.

Equilibrium dissociation constants (K_d) and fluorescence changes (F_+/F_-) upon nucleotide binding were determined by fluorescence titration as shown in Figure 1. Data were obtained at 20 °C in 30 mM Tris.HCl pH 7.5, 3 mM MgCl₂, 5 μM BSA and 25 mM KCl or 150 mM KCl where indicated.

Nucleotide	5-ATR-ParM		6-ATR-ParM	
	F_+/F_-	K_d (μM)	F_+/F_-	K_d (μM)
GDP	10.6	75.0	9.5	91.2
GDP (150 mM KCl)	11.7	45.8	10.1	48.5
ADP*	14.9	30.2	14.5	37.0
ADP (150 mM KCl)*	15.2	15.3	12.3	15.8
dGDP	9.0	105	8.7	149
dADP	13.1	27.5	12.2	41.7
CDP	9.5	826	4.8	760
dCDP	10.6	707	7.4	>1000
UDP	11.6	101	7.2	96.4
TDP	14.1	29.0	15.1	45.0

* Values are from reference [12].

FIGURE LEGENDS

Figure 1: Affinity of the biosensor for guanine nucleotides. 0.5 μM 5-ATR-ParM was titrated with GDP (circles) or GTP (squares) under two different salt conditions, 25 mM KCl (closed symbols) or 150 mM KCl (open symbols) in 30 mM Tris-HCl pH 7.5, 3 mM MgCl_2 and 5 μM BSA at 20 °C. Rhodamine fluorescence was excited at 553 nm and emission was recorded at 577 nm. Dissociation constants for GDP, obtained from hyperbolic curve fits, are summarized in Table 1.

Figure 2: Kinetics of GDP binding to the biosensor. (A) Fluorescence time courses after mixing 0.1 μM 5-ATR-ParM with increasing concentrations of GDP in a stopped-flow apparatus. Micromolar GDP concentrations are indicated in the figure. All concentrations are those in the mixing chamber. Fluorescence was excited at 546 nm and emission was detected after a 570 nm long pass filter. Data were analysed by single exponential curve fitting yielding the observed rate constants k_{obs} . (B) Plot of k_{obs} versus GDP concentration for 5-ATR- (open circles) and 6-ATR-ParM (closed circles). Association (k_{on}) and dissociation rate constants (k_{off}) were obtained from linear regression analysis. For 5-ATR-ParM k_{on} is 0.047 $\mu\text{M}^{-1}\text{s}^{-1}$ and k_{off} is 4.8 s^{-1} ; for 6-ATR-ParM k_{on} is 0.029 $\mu\text{M}^{-1}\text{s}^{-1}$ and k_{off} is 3.2 s^{-1} . Experiments were performed in 30 mM Tris-HCl pH 7.5, 25 mM KCl, 3 mM MgCl_2 and 5 μM BSA at 20 °C.

Figure 3: Assay of the GTPase activity of hGBP5. (A) Calibration of the fluorescence signal of the biosensor. 0.25 μM 5-ATR-ParM was titrated with GDP in the absence of GTP (open squares), with 0.5 mM (closed circles) or with 1 mM GTP (open circles) and fluorescence emission was monitored as in Figure 1. The slopes from linear regression analysis are 6.3 μM^{-1} , 6.1 μM^{-1} and 5.8 μM^{-1} at 0, 0.5 and 1 mM GTP, respectively. (B) Kinetics of GTP hydrolysis catalyzed by hGBP5 were measured under steady-state conditions with 0.22 μM hGBP1, different concentrations of GTP and 0.25 μM 5-ATR-ParM. The inset shows time courses of GDP formation at 0, 10, 20, 35, 50, 100, 150, 200 and 1000 μM GTP. Initial rates were determined by linear fits to data points below 10% turnover and are plotted versus GTP concentration. A hyperbolic curve fit yields the Michaelis-Menten parameters $K_{\text{M}} = 79 \mu\text{M}$ and $v_{\text{max}} = 0.467 \mu\text{M min}^{-1}$. Measurements were performed in 50 mM Tris-HCl pH 8.0, 25 mM KCl, 5 mM MgCl_2 , 2 mM DTT and 5 μM BSA at 25 °C.

Figure 4: Sos-catalyzed nucleotide exchange of Ras. (A) GDP to GTP exchange at different concentrations of Sos^{cat} . 10 μM Ras-GDP and 0.25 μM 5-ATR-ParM were incubated in the cuvette before GDP dissociation was initiated by the addition of 1 mM GTP and/or Sos^{cat} at the concentration indicated in the figure. The concentration of free GDP was calculated from a calibration as in Figure 4A. (B) GDP to GTP exchange at different concentrations of Ras-GDP. The experiment was performed as in (A) but with constant 25 nM Sos^{cat} and varying concentrations of Ras-GDP. The inset shows time courses of GDP dissociation at 0, 25, 50, 75, 100, 150, 200, 300 and 500 μM Ras-GDP. Initial rates were determined by linear regression and plotted versus Ras-GDP concentration. The solid line represents the hyperbolic fit to the experimental data. Measurements were performed in 20 mM Hepes pH 7.4, 150 mM KCl, 5 mM MgCl_2 , 2 mM DTT and 5 μM BSA at 25 °C.

Figure 1

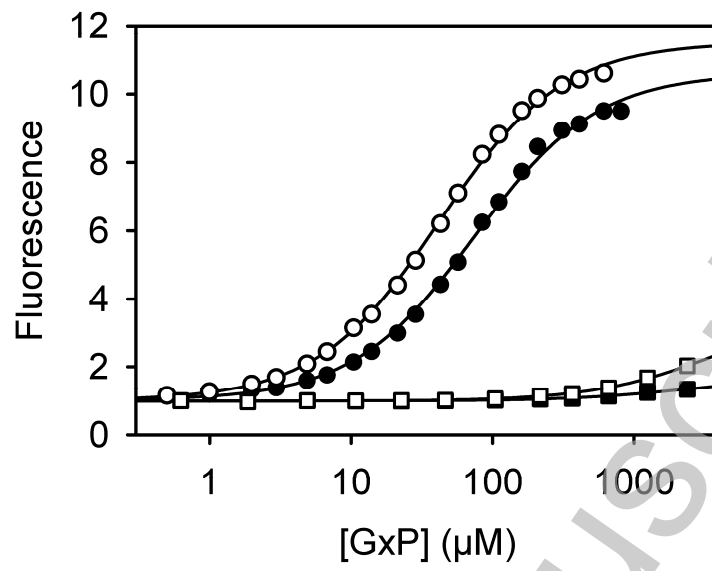
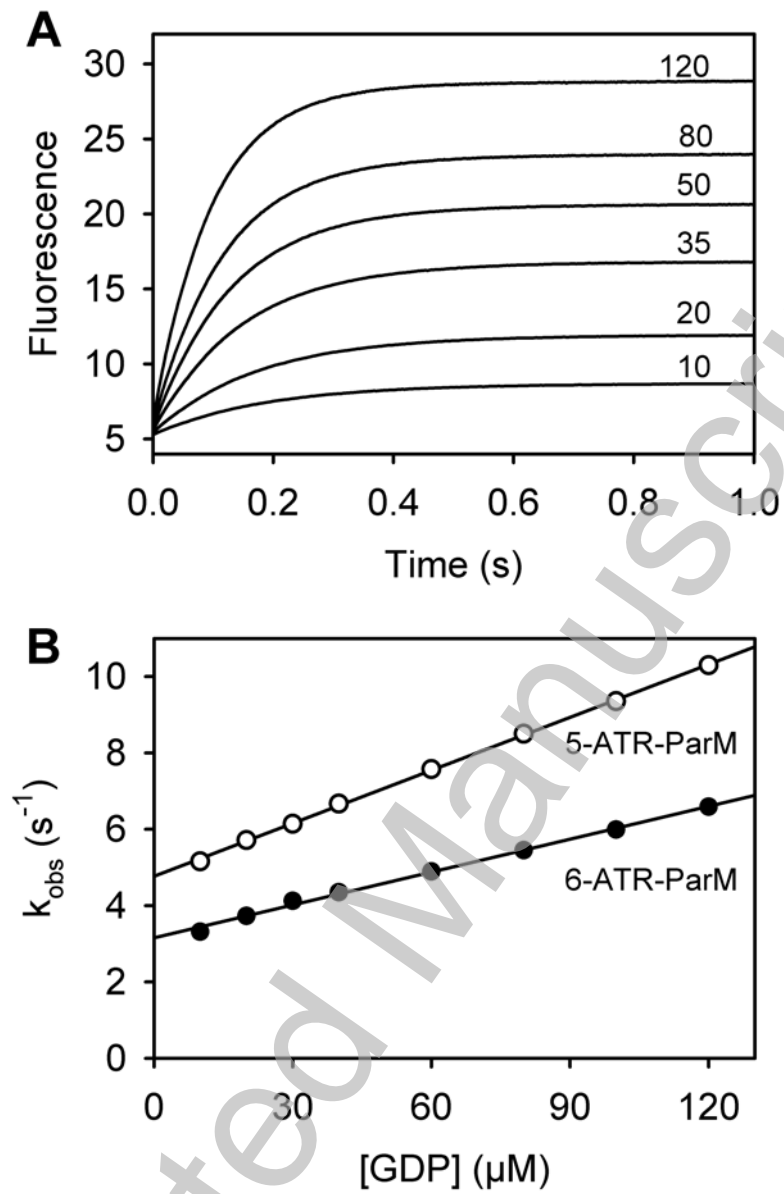
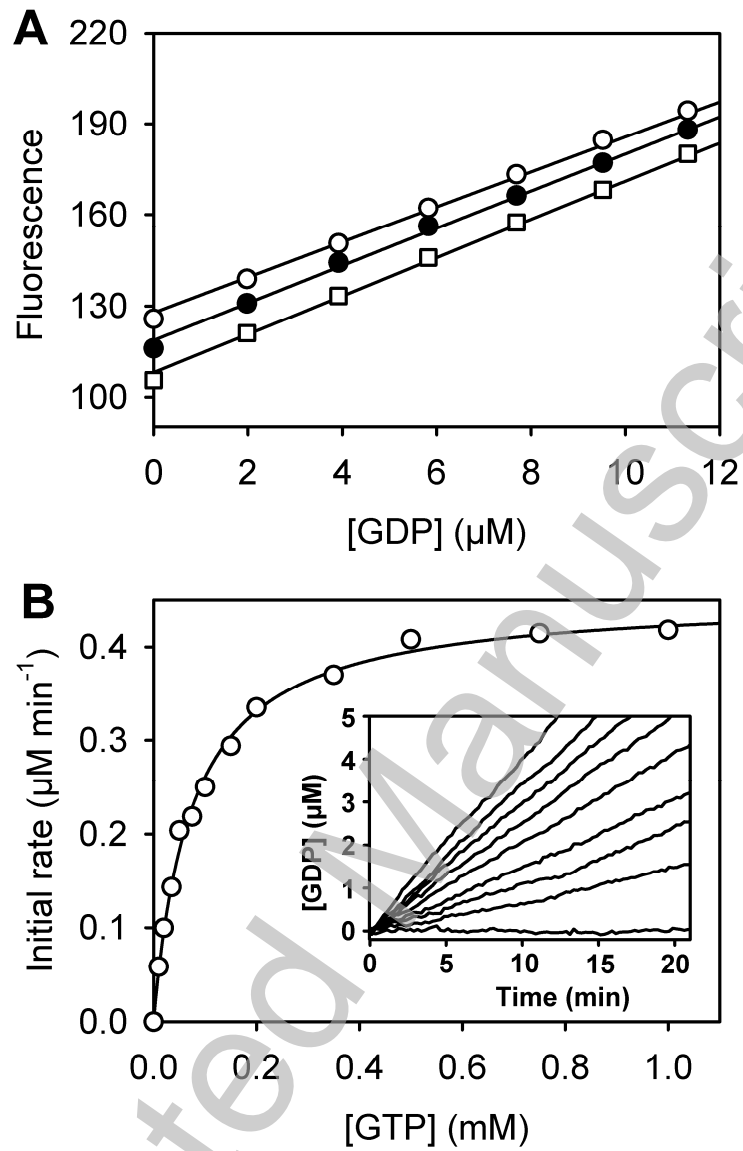


Figure 2



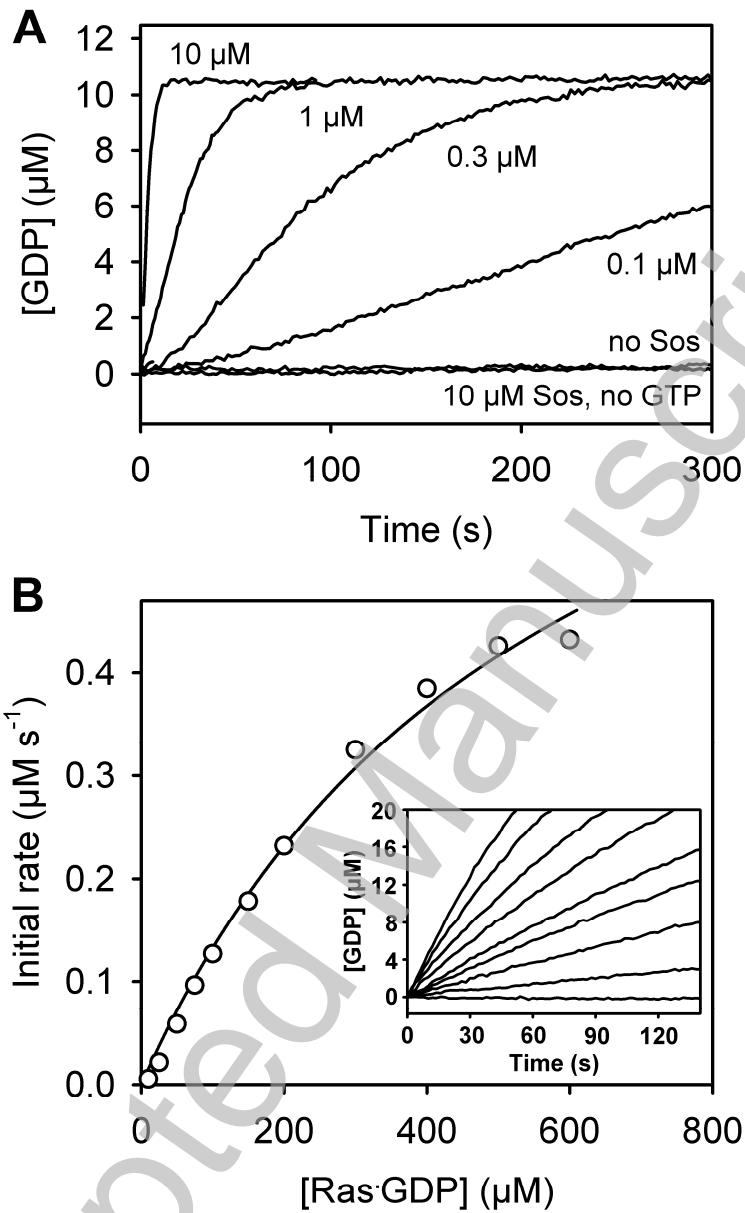
Accepted Manuscript

Figure 3



Accepted Manuscript

Figure 4



THIS IS NOT THE VERSION OF RECORD - see doi:10.1042/BJ20110349

Accepted Manuscript